

Near-infrared and X-ray obscuration to the nucleus of the Seyfert 2 galaxy NGC 3281

Chris Simpson

Subaru Telescope, National Astronomical Observatory of Japan, 650 N. A‘Ohōkū Place,
Hilo, HI 96720

ABSTRACT

We present the results of a near-infrared and X-ray study of the Seyfert 2 galaxy NGC 3281. Emission from the Seyfert nucleus is detected in both regions of the electromagnetic spectrum, allowing us to infer both the equivalent line of sight hydrogen column density, $N_{\text{H}} = 71.0^{+11.3}_{-12.3} \times 10^{26} \text{ m}^{-2}$ and the extinction due to dust, $A_V = 22 \pm 11$ magnitudes (90% confidence intervals). We infer a ratio of N_{H}/A_V which is an order of magnitude larger than that determined along lines of sight in the Milky Way and discuss possible interpretations. We consider the most plausible explanation to be a dense cloud in the foreground of both the X-ray and infrared emitting regions which obscures the entire X-ray source but only a fraction of the much larger infrared source.

Subject headings: galaxies: active — galaxies: individual (NGC 3281) — galaxies: nuclei — galaxies: Seyfert — infrared: galaxies — X-rays: galaxies

1. Introduction

In the current paradigm for the unification of Seyfert galaxies (see, e.g. Antonucci 1993), Seyfert 1 and Seyfert 2 galaxies are intrinsically the same object, the observed differences being due to significant obscuration along the line of sight to the nucleus in the latter class. This obscuration blocks the broad line region (BLR) and nuclear continuum source from view, leaving only the narrow lines clearly visible to indicate the presence of nuclear activity. Evidence to support this picture has come from many different areas, including spectropolarimetry (e.g. Antonucci & Miller 1985; Miller & Goodrich 1990), X-ray spectroscopy (Awaki et al. 1991; Turner et al. 1997a, 1997b, 1998), and near-infrared spectroscopy (Blanco, Ward & Wright 1990; Goodrich, Veilleux & Hill 1994), and it is now almost universally accepted.

The material responsible for obscuring the Seyfert nucleus lies preferentially in the equatorial plane of the AGN (whose axis is defined by the radio jets), and for this reason it is commonly referred to as the “torus”. Goodrich et al. (1994) have commented that measuring the line of sight opacity in a large sample of Seyfert galaxies could allow information to be gleaned about the torus’ geometry. Such measurements can be made at both near-infrared and X-ray wavelengths; the former observations determine the amount of dust along the line of sight, while the latter measure the photoelectric absorption column which can be converted into an equivalent hydrogen column density if the elemental abundances are known. Although it is believed that the X-rays are produced close to the black hole, and the near-infrared radiation comes from hot dust further out, the lines of sight to the two continuum sources should be similar since the BLR clouds have a low covering factor ($\lesssim 10\%$; e.g. Oke & Korycansky 1982; Shields, Ferland & Peterson 1995). Goodrich et al. (1994) state that it should therefore be possible to combine near-infrared and X-ray column measurements in a statistical manner if the gas-to-dust ratio (or, more correctly, the ratio of effective hydrogen column density to visual extinction, N_{H}/A_V) along the line of sight is shown to have the Galactic value of $N_{\text{H}}/A_V = 1.9 \times 10^{25} \text{ m}^{-2} \text{ mag}^{-1}$ (Bohlin et al. 1978, assuming $R \equiv A_V/E(B - V) = 3.1$).

Preliminary evidence favoring a universal value of the N_{H}/A_V ratio has come from detailed studies of two active galaxies, IC 5063 (Simpson, Ward & Kotilainen 1994) and Cygnus A (Simpson 1994a; Ward 1996). In both cases the derived values of N_{H} and A_V were found to have a similar ratio to Galactic lines of sight. However, Alonso-Herrero, Ward & Kotilainen (1997) have analyzed a sample of Seyfert 2 galaxies and found that the ratio can often be much larger. Unfortunately, the infrared data available to Alonso-Herrero et al. were of lower quality than those used in the studies by Simpson and colleagues, and their results are therefore less certain. High-quality data on a large sample of galaxies should produce a more conclusive result.

In this paper, we present a thorough near-infrared and X-ray study of the nucleus of the Seyfert 2 galaxy NGC 3281, and find that the N_{H}/A_V ratio along our line of sight which is more than an order of magnitude greater than the Galactic value. We investigate possible interpretations of this result. Throughout this paper we adopt a recession velocity with respect to the Galactic Standard of Rest for NGC 3281 of 3224 km s^{-1} (de Vaucouleurs et al. 1991). With a Hubble constant $H_0 = 50 \text{ km s}^{-1} \text{ Mpc}^{-1}$, our assumed distance is 64.5 Mpc .

2. The infrared images

2.1. Observations

NGC 3281 was observed using the IRAC-1 infrared array camera on the European Southern Observatory 2.2 m telescope at La Silla, Chile, on the night of UT 1994 Dec 17. Images were taken in the J , H , and K filters, with on-source integration times of 180 s at J and H , and 240 s at K . An equal amount of time spent on regions of sky $2'$ away, and these images were used to flatfield and sky-subtract the images of the galaxy. Since the conditions were non-photometric during the observations, we have flux calibrated our images from the aperture photometry of Glass & Moorwood (1985). We use their $12''$ aperture fluxes, since these will be less affected by possible variability of the Seyfert nucleus. However, we note that our data have the same ratio of $12''$ to $6''$ aperture fluxes as those of Glass & Moorwood, so there appears to be no significant variability between the two epochs.

Further infrared images of NGC 3281 were taken with IRCAM3 on the 3.8 m United Kingdom Infrared Telescope (UKIRT) at the summit of Mauna Kea, Hawaii, on UT 1996 Jan 5, a few days prior to our *ASCA* observation (§3.2). Two 60 s images were taken in the K filter, one centered on NGC 3281, and one on a nearby blank region of sky. Images were also taken in the L' and M filters, totaling 300 s on source and 300 s on neighboring patches of sky, to enable flatfielding. Flux calibration was performed using observations of UKIRT photometric standards over the course of the night. Simulated aperture photometry of our K image agrees to within 5% with that of Glass & Moorwood (1985).

2.2. Separation of galaxy and nucleus

We have used two different procedures to measure the fluxes of a possible unresolved nuclear source in the infrared images since the relative contributions of nucleus and host galaxy vary greatly with wavelength. To determine the nuclear flux at H and K in the ESO images, we subtracted the ESO J image from the images in these filters, after scaling it so that the counts matched in an annulus $3'' < r < 5''$, and then performed photometry in a $3''$ aperture on the residual unresolved source. We opt for this method rather than the profile fitting advocated by Simpson (1994b) because of the small field of view of IRAC-1 and the uncertain sky level. The nuclear excess is clearly visible in radial surface brightness profiles, and the correction needed account for the presence of color gradients which caused Simpson to disfavor this method is small for a galaxy as extended as NGC 3281. At L' and M , the host galaxy is not detected with any significance, so we have performed photometry within a $3''$ aperture, and corrected our measurements for contamination from the underlying host galaxy using the spectrum of β Peg (Strecker, Erickson & Witteborn 1979), an M2 II–III star whose infrared colors match those of the normal ellipticals in the sample of Frogel

et al. (1978). We estimate that the host galaxy contributes only 10% and 2% of the flux within the $3''$ aperture at L' and M respectively, and our nuclear magnitudes are therefore insensitive to the assumed galaxy colors. We have also used the aperture photometry of Glass & Moorwood (1985) to determine the strength of the nuclear source at L , performing a similar analysis to that used on the ESO data. We present the results of the photometry in Table 1.

2.3. Extinction to the nucleus

Studies of large samples of quasars (e.g. Neugebauer et al. 1987) have shown that the near-infrared continuum is a power law with spectral index $\alpha = 1.4 \pm 0.3$ ($S_\nu \propto \nu^{-\alpha}$), believed to be due to thermal emission from hot dust at a range of temperatures. Seyfert galaxies are believed to be merely scaled-down versions of quasars and their near-infrared continua should be similar. Fadda et al. (1998) find slightly steeper values for Seyfert 1s ($\alpha \approx 1.7$ – 2.0), although this is quite critical on the separation of host galaxy and nucleus at the shorter wavelengths. We assume that the intrinsic near-infrared continuum of NGC 3281 is also well described by a power law and perform a grid search in the spectral index–reddening plane to determine what values of α and the nuclear extinction produces the best fit to the observed nuclear magnitudes. We use the interstellar extinction law of Rieke & Lebofsky (1985), and find that $A_V = 22 \pm 11$ and $\alpha = 1.95_{-1.40}^{+1.30}$ (90% confidence intervals). As Figure 1 shows, the two parameters are strongly anti-correlated, since increased extinction has the effect of steepening the spectrum. The best-fitting reddened power law model is shown in Figure 2.

An additional consistency check can be made using the observed strength of the [O III] $\lambda 5007$ emission line, which is an isotropic indicator of the strength of the Seyfert nucleus (see Mulchaey et al. 1994). Since Seyfert galaxies are believed to be merely scaled-down versions of radio-quiet quasars, we use the equivalent width of 24 \AA (with scatter of a factor 2) for this line in the bright quasar sample (Miller et al. 1992) to estimate the unobscured optical continuum level for the isolated Seyfert nucleus (since Miller et al. observed bright quasars, the contamination by starlight from the host galaxy will be small and hence their measurement of the equivalent width is an indication of the line strength relative to the non-stellar continuum alone). The integrated flux of $f_{[\text{O III}]} = 1.0 \times 10^{-15} \text{ W m}^{-2}$ measured by Storchi-Bergmann, Wilson & Baldwin (1992b) then implies a continuum flux at 5007 \AA of $4.2 \times 10^{-17} \text{ W m}^{-2} \text{ \AA}^{-1}$, uncertain by a factor of 2. By adopting the mean optical–near-infrared quasar spectrum from Neugebauer et al. (1987), we determine an unobscured nuclear magnitude of $K = 9.33 \pm 1.08$, implying an

extinction $A_K = 3.00 \pm 1.08$, or $A_V = 27 \pm 10$. The good agreement between this number and our near-infrared color analysis adds further weight to our interpretation of the nuclear source in NGC 3281 as a reddened Seyfert nucleus.

The above analysis has implicitly assumed that the emission arises in a single region of negligibly small optical depth, seen through a foreground screen. However, since the longer wavelength emission is emitted by cooler dust located further from the nucleus, it will provide additional obscuration along the line of sight to the hotter dust closer to the nucleus. One might therefore expect the foreground screen model to fit the data poorly, either underestimating the longer wavelength fluxes or overestimating the shorter wavelength emission. We briefly show here that the optical depth of the near-infrared emitting region is too small to have a significant effect.

Following Barvainis (1987), if the dust has a temperature T_i at the inner edge of the torus, radius r_i , then the optical depth at ultraviolet wavelengths from the nucleus to some radius $r > r_i$ where the dust temperature is T is given by

$$\tau_{UV} = 5.6 \ln(T_i/T) + 2 \ln(r_i/r).$$

The second term on the right hand side is always negative (since $r > r_i$), so $\tau_{UV} < 5.6 \ln(T_i/T)$. The longest wavelength we have studied is $4.8 \mu\text{m}$, which is the peak wavelength for dust at a temperature of 600 K. We take T_i to be 1500 K (Barvainis 1987), hence $\tau_{UV} \approx 5$ at the $4.8 \mu\text{m}$ -emitting region. Making the same assumptions about the heating continuum as Storchi-Bergmann et al. (1992a,b), this optical depth can be achieved with as little as 5 mag of visual extinction, which is similar to our uncertainty and much lower than the column we derive. It is therefore not surprising that a simple foreground screen model provides an acceptable fit to the observations.

It can also be shown straightforwardly that a collection of sources emitting the same spectrum, but viewed through different amounts of extinction, cannot combine to mimic a foreground screen. While it is true that several sources emitting *different* spectra, and seen through different extinctions, could achieve this feat, it is not only contrived but cannot explain the low dispersion observed in the near-infrared spectral indices of quasars and Seyfert 1 galaxies. In these objects, the near-IR emission is seen effectively unobscured and, if this emission is produced by a number of sources with different spectral shapes, it is unclear how these could always combine to produce the same overall spectrum. Rather, the emission must come from a single, coherent region. Our interpretation of the nuclear source in NGC 3281 as a Seyfert 1-like nucleus seen through $A_V \approx 22$ mag of foreground extinction is therefore the most plausible explanation.

3. The X-ray data

3.1. Previous X-ray observations

NGC 3281 appears in the *Ariel V* catalogue (McHardy et al. 1981) as the proposed identification for the source 3A 1030–346. Since the error box is approximately 1.8 deg^2 , this identification cannot be considered secure, although the 2–10 keV flux of $(2.9 \pm 0.6) \times 10^{-14} \text{ W m}^{-2}$ implies a ratio of [O III] to hard X-ray flux typical of Seyfert galaxies (Mulchaey et al. 1994). However, a source with a flux of $(3.6 \pm 0.4) \times 10^{-14} \text{ W m}^{-2}$ was detected by *HEAO A-1* (1H 1027–351; Wood et al. 1984), and although its error box overlaps with that of 3A 1030–346, it does *not* include NGC 3281. Since *HEAO A-1* had greater spectral coverage and higher sensitivity than *Ariel V*, it should have detected all the sources in the *Ariel V* catalog. Given the consistent flux measurements and positions of 3A 1030–346 and 1H 1027–351, we propose that these sources are the same, as yet unidentified (to the best of our knowledge), X-ray source located within the region of overlap between their two error boxes. Neither of them should be identified with NGC 3281.

Consistent with this interpretation is a pointed observation made with the IPC on board the *Einstein* satellite (Fabbiano, Kim & Trinchieri 1992). The upper limit to the count rate of $0.017 \text{ counts s}^{-1}$ is an order of magnitude lower than that expected if NGC 3281 has a ratio of intrinsic 2–10 keV to [O III] luminosities typical of Seyferts, and is seen through a column density $N_{\text{H}} = 5.3 \times 10^{26} \text{ m}^{-2}$ (corresponding to $A_V = 28 \text{ mag}$ and the N_{H}/A_V ratio of Bohlin et al. 1978). It is possible that NGC 3281 is a relatively feeble emitter of X-rays, but since the bandpass of the *Einstein* IPC is fairly soft (0.16–3.5 keV), the observed flux is highly dependent on the amount of photoelectric absorption, and a large absorbing column might be the culprit.

3.2. ASCA Observations and reduction

The *ASCA* X-ray satellite was used to observe NGC 3281 on UT 1996 Jan 8, to determine the intrinsic X-ray luminosity and photoelectric absorbing column. The SIS detectors operated in 1-CCD faint mode, and the GIS detectors in PH mode. Standard screening criteria were used to exclude periods of bad data. The raw data were screened to exclude events detected while the telescope was pointing within 10° of the Earth, and those detected within 60 s of a passage through the South Atlantic Anomaly or within 60 s of a day/night transition. Data taken with the GIS detectors when the cut-off rigidity (COR) was below $7 \text{ GeV}/c$, or with the SIS when the COR was below $6 \text{ GeV}/c$, were also excluded. Finally, events detected by the SIS when the telescope was pointing within 20° of the

sun-illuminated Earth were also excluded. After performing this screening, light curves were produced which revealed a few short periods of observation, sandwiched between longer periods of rejected data, when the background was unstable and unusually high. These short periods of unstable background, totaling approximately 500 s, were also excluded from the analysis. The total exposure times in the four detectors after screening are listed in Table 2.

We converted our SIS data to bright mode to allow us to use the archived high signal-to-noise ratio blank sky observations for background subtraction, and used the same extraction regions for both the source and sky. We used the minimum recommended extraction regions (3' for the SIS detectors, 4' for the GIS detectors) where possible, since the source was faint and unresolved. For the SIS1 detector, however, this aperture extended beyond the edge of the CCD and we were therefore obliged to use a slightly smaller aperture (2'8).

As is the norm for the modeling of X-ray spectra, the observed data were compared to a model spectrum which had been convolved with the detector response matrix, using the χ^2 statistic to quantify the quality of fit. We used the SIS energy response matrices of 1994 Nov 9, and the GIS response matrices of 1995 Jun 3. In addition, to avoid the difficulties of error determination when dealing with small number statistics, the observed data were regrouped so that each bin contained at least 20 events, and channels containing no events were flagged as bad and not used in determining the best fit. In addition, the GIS channels with energies below 0.9 keV and the SIS channels with energies above 8 keV were also excluded due to their poor sensitivities and tendency to be affected by non-random errors.

3.3. Analysis

The X-ray continuum of a typical active galactic nucleus (see Mushotzky, Done & Pounds 1993) can be modeled as a power law with photon index $\Gamma \approx 1.9$ plus a reflection hump. In low-quality data such as ours, the sum of these components resembles a flatter power law with $\Gamma \approx 1.7$. The spectrum is modified by photoelectric absorption (both from the Milky Way and the host galaxy) and also features a $K\alpha$ emission line of iron with a rest energy of 6.4 keV and an intrinsic rest frame equivalent width of 100–200 eV (Mushotzky et al. 1993; Nandra et al. 1997). In addition, there may be a significant fraction of the continuum which is spatially extended or scattered into our line of sight, and thus avoids the heavy absorption from the torus that surrounds the nucleus. In such cases, the spectrum will have two absorption cutoffs: one at a high energy associated with the torus and one at a low energy associated with the much smaller gas column through the host

galaxy and Milky Way. NGC 4945 (Done, Madejski & Smith 1996) is a good example of such an object, and NGC 3281 possesses a very similar X-ray spectrum, which we therefore modeled in a similar manner.

We performed our analysis with the XSPEC package (Shafer et al. 1994), which uses the Morrison & McCammon (1983) cross-sections for photoelectric absorption. Since the power law observed at low energies is merely an extended or reflected component of the second power law, we constrained them to have the same photon index. We also fixed the column density obscuring the scattered/extended continuum at the Galactic value of $N_{\text{H}} = 6.4 \times 10^{24} \text{ m}^{-2}$ (Heiles & Cleary 1979). This model gave an acceptable fit ($\chi^2_{\nu} = 1.06$ with 73 degrees of freedom), although the parameters are not particularly well constrained due to the low count rate. The best fit values for the photon index, equivalent hydrogen column density along the line of sight to the transmitted component, and equivalent width of the Fe $K\alpha$ line, together with their associated 90% confidence intervals are presented in Table 3. We show the grouped data and best-fit models for the SIS0 and GIS3 detectors in Figure 3. The Fe $K\alpha$ line is unresolved in all the fits, although our relatively poor signal-to-noise ratio does not exclude the possibility of a fairly significant broad component, such as that seen by Turner et al. (1998).

There is an excess of counts above our best fitting models in both SIS detectors in the range 0.7–1 keV. A similar excess has also been seen in the Seyferts Mrk 3 and NGC 1365 (Turner, Urry & Mushotzky 1993) and the LINERs NGC 2639 (Reichert, Mushotzky & Filippenko 1994) and possibly NGC 4639 (Koratkar et al. 1995). Turner et al. (1993) speculatively attributed this excess to an emission-line complex of Fe L and ionized oxygen. Such an explanation might also apply to NGC 3281, although the sensitivities of the GIS detectors at these energies are insufficient to determine whether this excess is present in all detectors or only in SIS0+SIS1, and might therefore be the result of poor background subtraction in these detectors. Whatever the cause, it is likely that this excess is artificially increasing the value of the photon index derived for the SIS spectra, so we have performed additional fitting using only the data in channels with energies above 1 keV. These results are also presented in Table 3 and Figure 4.

Figure 5 shows confidence level contour plots for the photon index and gas column density. It is clear from these figures that the overall consistency of the fits between the different detectors is increased when the data below 1 keV is excluded. We therefore choose to use the results from fits to the $E > 1 \text{ keV}$ data only, after noting that the parameter we are most interested in (the depth of the intervening gas column) is constrained by the position of the cutoff at $\sim 5 \text{ keV}$ and is thus largely unaffected by the inclusion or exclusion of the low energy data.

We investigated alternative models to see whether they were able to provide acceptable fits to our data. We added a Compton reflection hump, which provides additional flux at $E \gtrsim 5$ keV and might therefore help to explain the change in flux which we have attributed to photoelectric absorption. This made no significant change to any of the fitting parameters, and in fact led to a worse quality of fit indicator by virtue of the many additional free parameters. We also added a thermal plasma, based on the calculations of Raymond & Smith (1977), as it could be responsible for the putative emission lines at soft energies. We find, however, that such a plasma does not provide significant flux in the 1–3 keV range, and contributes negligibly at higher energies. It can therefore have little or no effect on the hydrogen column density we derive, which Table 3 shows remains fairly constant over a large range of photon indices.

The observed 2–10 keV flux of the best fitting model is $2.7 \times 10^{-15} \text{ W m}^{-2}$, more than an order of magnitude fainter than the source(s) detected by *Ariel V* and *HEAO A-1*. This supports the assertion that the detections made by these satellites are of a separate and presumably unrelated source. The intrinsic 2–10 keV flux (i.e. in the absence of the large absorbing column) is $2.3 \times 10^{-14} \text{ W m}^{-2}$, so the ratio of [O III] to hard X-ray flux is within the 1σ scatter for Seyfert galaxies (Mulchaey et al. 1994), and the absorption-corrected luminosity $L_{2-10\text{keV}} = 1.1 \times 10^{36} \text{ W}$ is typical of Seyfert galaxies. The few other Seyfert 2s known with similarly large absorption columns ($N_{\text{H}} \gtrsim 10^{28} \text{ m}^{-2}$; e.g. NGC 1068, NGC 4945) show large Fe K α equivalent widths, apparently because the continuum photons are preferentially absorbed over the line photons. Although the uncertainties on the equivalent width of the Fe K α line are large, our derived value of ~ 500 eV is larger than typical values, and so NGC 3281 falls naturally into this picture. Our model therefore not only provides an acceptable fit to the data, but also suggests that the intrinsic X-ray spectrum of NGC 3281 is that of a typical Seyfert galaxy.

4. Discussion

In §2 we showed that the near-infrared properties of the unresolved nuclear source in NGC 3281 are consistent with a normal Seyfert 1 spectrum seen through $A_V = 22 \pm 7$ mag (1σ error) of extinction. In §3 we showed that NGC 3281’s X-ray properties are consistent with a normal Seyfert 1 spectrum seen through an equivalent hydrogen column of $N_{\text{H}} = (7.1 \pm 1.2) \times 10^{27} \text{ m}^{-2}$ (1σ error). Taken together, the ratio of gas to dust columns, $N_{\text{H}}/A_V = (3.2 \pm 1.7) \times 10^{26} \text{ m}^{-2} \text{ mag}^{-1}$ (90% confidence), is more than an order of magnitude larger than the Galactic ratio derived by Bohlin et al. (1978) of $1.9 \times 10^{25} \text{ m}^{-2} \text{ mag}^{-1}$. The implication of this is fairly obvious, i.e. that extinction estimates from near-infrared and

X-ray analyses cannot be combined in the manner hoped for by Goodrich et al. (1994).

We doubt that the apparent dearth of dust along our line of sight to the nucleus is because NGC 3281 has a low dust content on a galactic scale. There is significant dust obscuration in the central 20 kpc of the galaxy (Storchi-Bergmann et al. 1992b), the stellar population of the bulge is typical of an early-type galaxy and the metallicity near the nucleus is estimated to be about twice solar, indicating a fairly normal course of stellar evolution. While it is true that our line of sight through the thick molecular torus in NGC 3281 is very unlike the Galactic lines of sight along which Bohlin et al. (1978) derived their N_{H}/A_V ratio, the analyses of IC 5063 (Simpson et al. 1994) and Cygnus A (Simpson 1994a) did not produce large N_{H}/A_V ratios. We cannot therefore make an arbitrary appeal to unusual physical conditions to explain the discrepancy, and must look for an alternative explanation.

We note that the high inclination of NGC 3281 means that the obscuring material may be part of a larger-scale structure in the plane of the galactic disk (McLeod & Rieke 1995; Simcoe et al. 1997). This does not affect the following discussion in any way, which relates to the quantities of gas and dust along the line of sight, and not to their locations.

4.1. An alternative origin for the hot dust

We first rule out the possibility that the near-infrared source we observe has some other origin than a reddened Seyfert 1 nucleus. The observed 1–5 μm luminosity of the source is $5 \times 10^9 L_{\odot}$, but its spectral index ($\alpha \approx 5$) is almost certainly too steep to be intrinsic, and the reddening requires that the true luminosity be higher. Blue intrinsic spectra, such as those appropriate for the Rayleigh-Jeans tail of a starburst, require a luminosity in excess of $10^{12} L_{\odot}$ in this wavelength region alone, and so the spectrum must be intrinsically red, or cool, to avoid such unreasonably large numbers. Thermal emission from dust is the only plausible candidate, requiring a luminosity of about $2 \times 10^{10} L_{\odot}$, which must also be the luminosity of the heating source. A powerful starburst is the only phenomenon, other than an active galactic nucleus, which can produce this quantity of radiation on a small scale, but while starbursts are frequently seen in active galaxies, they tend to exist in kpc-scale rings, and the unresolved nature of the source we observe requires the burst to be occurring on a scale an order of magnitude smaller, despite having a comparable luminosity. A more serious problem with a starburst as the heating source is that the dust must lie close to the individual stars for it to be heated to temperature of $\gtrsim 1000$ K. A single dust shell around a cluster of a few million O stars will not work. Yet we know that the good fit we obtain to the data with a simple foreground screen model precludes a geometry where the dust is

clumped around the stars and suffers a large range of extinctions.

4.2. Supersolar metallicity

Although we quote equivalent hydrogen columns, our measurement of the photoelectric absorption column has been determined by the cutoff at ~ 5 keV, where the total photoelectric absorption cross section is dominated by heavy elements. The optical depth at this energy is therefore a measure of the metal abundance along the line of sight, and by assuming solar metallicity we overestimate the true hydrogen column density, N_H , by a factor approximately equal to the metallicity (relative to solar)¹. If the abundances of these elements are enhanced by a factor of ~ 10 above solar, the *true* hydrogen column density would be in line with the near-infrared extinction.

It is known that some heavy elements (most notably N and O) have high abundances in the centers of early-type spirals (e.g. Storchi-Bergmann, Wilson & Baldwin 1996), but they are typically no more than a factor of 3–4 above solar. In addition, other elements need not be overabundant since the enrichment of nitrogen and oxygen is usually explained by the CNO cycle. Quadrupling the N and O abundances alone increases the photoelectric absorption cross-section at 6.4 keV by less than a factor of two. While the very high metallicity required need only exist within the torus, it is unclear how such a confinement might occur, and more importantly why a similar effect was not observed in either IC 5063 or Cygnus A. While we may have overestimated the hydrogen column density by a factor of about two (spectroscopy of the narrow line gas indicates $Z \approx 2Z_\odot$; Storchi-Bergmann et al. 1992b), we have not done so by the order of magnitude necessary to bring it in line with the dust column.

4.3. A dense obscuring cloud

Since both columns we have measured appear to be true representations of the amount of material along the lines of sight, we explore a geometric interpretation which exploits the fact that the near-infrared and X-ray sources are not cospatial. Perhaps the most natural explanation is that a BLR cloud lies along the line of sight to the X-ray emitting region. This could contribute significantly to the photoelectric absorbing column, but would not

¹Most of the opacity is provided by O, Si, S and the Fe L-shell, so it is the abundances of these elements which most strongly determine the effective column density.

affect the extinction to the hot dust since the BLR is located closer to the nucleus and therefore not in the dust’s foreground. Unfortunately, the time for a cloud with velocity 10^4 km s^{-1} to traverse the BLR is only about one year (Wanders et al. 1995), yet the extra photoelectric absorption must have been present at the times of the three previous X-ray observations. The low covering factor of BLR clouds appears to exclude the possibility of a transient phenomenon like this occurring at four separate observational epochs. On the other hand, if BLR clouds have a larger covering factor cover a small range of solid angle (e.g. close to the equatorial plane), and our line of sight passes through this region, the probability would be larger. For the probability of a BLR cloud to lie along our line of sight on four separate occasions to be significant, however, the probability of a cloud to obscure the X-ray nucleus on any single occasion must be fairly large, and therefore we should expect analyses such as the one we perform here to frequently produce large N_{H}/A_V ratios, again at odds with the results for IC 5063 and Cygnus A.

A cloud located in front of both emission regions can provide an explanation. Since the X-rays come from a much smaller region than do the near-infrared photons, a cloud could completely cover the X-ray source and yet still permit an unobscured view of much of the infrared-emitting region. If such a cloud were sufficiently optically thick to block out all near-infrared radiation beyond it, even at $5 \mu\text{m}$, we would only detect the emission from the unobscured regions, and hence derive a low extinction. This situation is shown schematically in Figure 6.

It is clear that for this picture to work, the cloud must be smaller than the size of the infrared-emitting region, which is set by the height of the inner regions of the torus. The inner radius of the torus, r , is determined by the location at which dust cannot exist in thermal equilibrium with the nuclear radiation field, and so its height, h , is given by

$$h \approx 2r \cot \theta_c = 0.5(\pi\sigma)^{-0.5} L^{0.5} (Q_a/Q_e)^{0.5} T_{\text{sub}}^{-2} \cot \theta_c,$$

where $\theta_c = 35^\circ$ is the half-opening angle of the ionization cone (Storchi-Bergmann et al. 1992b), $L = 8 \times 10^{36} \text{ W}$ is the heating luminosity of the nucleus, $Q_a/Q_e = 100$ is the ratio of the dust optical absorption to infrared emission coefficients and $T_{\text{sub}} = 1500 \text{ K}$ is the sublimation temperature of dust. The torus is therefore $\sim 0.7 \text{ pc}$ in height, and for a spherical cloud to be smaller than this yet still produce most of the observed photoelectric absorption, its density must be $n_{\text{H}} \gtrsim 3 \times 10^{11} \text{ m}^{-3}$. Although large, this is only two orders of magnitude larger than the mean density needed to produce a Compton-thick torus smaller than 100 pc , and it is therefore not unreasonable to believe that such dense condensations could exist. In fact, it might be more accurate to consider such condensations as inhomogeneities, rather than *bona fide* clouds.

Because this cloud lies further from the nucleus than do the BLR clouds, it will be

moving more slowly and the increased absorption will persist over a much longer timescale,

$$t \sim 1300 \left(\frac{d_c}{0.7 \text{ pc}} \right) \left(\frac{v}{300 \text{ km s}^{-1}} \right)^{-1} \text{ yr.}$$

It is therefore entirely plausible that such a cloud could have obscured the X-ray source during all four observations. Indeed, we would expect the strong X-ray absorption to persist for many years to come.

5. Summary

We have presented a detailed near-infrared and X-ray analysis of the Seyfert 2 galaxy NGC 3281. We have shown that its near-infrared and X-ray properties, taken separately, are unremarkable and support the standard unification model for Seyfert galaxies where Seyfert 2s are simply Seyfert 1 galaxies seen through significant obscuration. However, the ratio of the gas and dust column densities we derive is $N_{\text{H}}/A_V = (3.2 \pm 1.7) \times 10^{26} \text{ m}^{-2} \text{ mag}^{-1}$ (90% confidence), more than an order of magnitude larger than the ratio derived by Bohlin et al. (1978) for lines of sight within the Milky Way. It is clear, therefore, that obscuring columns derived from near-infrared and X-ray observations cannot be arbitrarily interchanged using a normal gas-to-dust ratio, as Goodrich et al. (1994) had suggested.

Although we cannot rule out unusual physical conditions in the torus of NGC 3281 as the cause for the large ratio, such conditions are not common to all tori, since previous studies of two other active galaxies (Simpson et al. 1994; Simpson 1994a) produced results consistent with the Galactic ratio. Among the alternatives we have investigated, we have ruled out a compact starburst and a BLR cloud lying along the line of sight. We cannot rule out high metallicity confined to the obscuring material, but consider it unlikely based on the IC 5063 and Cygnus A results. Our preferred explanation is an optically thick cloud which obscures the entire X-ray source but only a fraction of the infrared source.

We are currently undertaking similar studies of many more Seyfert 2 galaxies in an attempt to learn more about the gas and dust obscuration. We have disfavored certain scenarios by virtue of their being unable to explain the IC 5063 and Cygnus A results, which we consider “normal”, yet with a sample of only three objects, it is perhaps premature to discuss what is and is not normal. In our preferred picture, we would expect most objects to possess a N_{H}/A_V ratio similar to the Galactic value, with the incidence of galaxies with large N_{H}/A_V ratios indicating the covering factor of the putative dense clouds, but a larger dataset may support a different picture. We will report on the results of this study in the near future.

This work has been supported by NASA grant number NAG 5-3393 from the *ASCA* Guest Observer Program. The United Kingdom Infrared Telescope is operated by the Joint Astronomy Centre on behalf of the U. K. Particle Physics and Astronomy Research Council. Count rates for the *Einstein* IPC were determined using the program PIMMS, obtained through the High Energy Astrophysics Science Archive Research Center Online Service, provided by the NASA-Goddard Space Flight Center. The author is extremely grateful to Andrew Wilson and Martin Ward for discussions during the writing of this paper, and to the referee, Mike Eracleous, for comments which have substantially improved its content. Parts of this work were performed at the Jet Propulsion Laboratory, California Institute of Technology, under a contract with the National Aeronautics and Space Administration.

REFERENCES

- Alonso-Herrero, A., Ward, M. J., Kotilainen, J. K. 1997, MNRAS, 288, 977
- Antonucci, R. 1993, ARA&A, 31, 473
- Antonucci, R. R. J., & Miller, J. S. 1985, ApJ, 297, 621
- Awaki, H., Koyama, K., Inoue, H., & Halpern, J. P. 1991, PASJ, 43, 195
- Barvainis, R. 1987, ApJ, 320, 537
- Biermann, P., & Harwit, M. 1980, ApJ, 241, L105
- Blanco, P. R., Ward, M. J., & Wright, G. S. 1990, MNRAS, 242, 4P
- Bohlin, R. C., Savage, B. D., & Drake, J. F. 1978, ApJ, 224, 132
- de Vaucouleurs, G., de Vaucouleurs, A., Corwin Jr, H. G., Buta, R. J., Paturel, G., & Fouqué, P. 1991, Third Reference Catalog of Bright Galaxies. Springer-Verlag.
- Done, C., Madejski, G. M., & Smith, D. A. 1996, ApJ, 463, L63
- Draine, B. T., & Lee, H. M. 1984, ApJ, 285, 89
- Fabbiano, G., Kim, D.-W., & Trinchieri, G. 1992, ApJS, 80, 531
- Fadda, D., Giuricin, G., Granato, G. L., & Vecchies, D. 1998, ApJ, 496, 117
- Frogel, J. A., Perrson, S. E., Aaronson, M., & Matthews, K. 1978, ApJ, 220, 75
- Glass, I. S., & Moorwood, A. F. M. 1985, MNRAS, 214, 429
- Goodrich, R. W., Veilleux, S., & Hill, G. J. 1994, ApJ, 422, 521
- Heiles, C., & Cleary, M. N. 1979, Aust. J. Phys. Suppl., 47, 1
- Koratkar, A., Deustua, S. E., Heckman, T., Filippenko, A. V., Ho, L. C., & Rao, M. 1995, ApJ, 440, 132
- Lightman, A. P., & White, T. R. 1988, ApJ, 335, 57
- Mathis, J. S., Rumpl, W., & Nordsieck, K. H. 1977, ApJ, 217, 425
- McHardy, I. M., Lawrence, A., Pye, J. P., & Pounds, K. A. 1981, MNRAS, 197, 893
- McLeod, K. K., & Rieke, G. H. 1995, ApJ, 441, 96
- Miller, J. S., & Goodrich, R. W. 1990, ApJ, 355, 456
- Miller, P., Rawlings, S., Saunders, R., & Eales, S. 1992, MNRAS, 254, 93
- Morrison, R., & McCammon, D. 1983, ApJ, 270, 119
- Mulchaey, J. S., Koratkar, A., Ward, M. J., Wilson, A. S., Whittle, M., Antonucci, R. R. J., Kinney, A. L., & Hurt, T. 1994, ApJ, 436, 586

- Mushotzky, R. F., Done C., & Pounds K. A. 1993, *ARA&A*, 31, 717
- Nandra, K., George, I. M., Mushotzky, R. F., Turner, T. J., & Yaqoob, T. 1997, *ApJ*, 477, 602
- Neugebauer, G., Green, R. F., Matthews, K., Schmidt, M., Soifer, B. T., & Bennett, J. 1987, *ApJS*, 63, 615
- Oke, J. B., & Korycansky, D. G. 1982, *ApJ*, 255, 11
- Raymond, J. C., & Smith, B. W. 1977, *ApJS*, 35, 419
- Reichert, G. A., Mushotzky, R. F., & Filippenko, A. V. 1994, in *The First ROSAT Symposium*, ed. E. M. Schlegel & R. Petre (New York: American Institute of Physics)
- Rieke, G. H., & Lebofsky, M. J. 1985, *ApJ*, 288, 618
- Shafer R. A., Haberl F., Arnaud K. A., Tennant A. F., 1994, *XSPEC: An X-Ray Spectral Fitting Package* (Greenebtl: Goddard Space Flight Center)
- Shields, J. C., Ferland, G. J., & Peterson, B. M. 1995, *ApJ*, 441, 507
- Simcoe, R., McLeod, K. K., Schachter, J., & Elvis, M. 1997, *ApJ*, 489, 615
- Simpson, C. J. 1994a, D.Phil. thesis, University of Oxford
- Simpson, C. 1994b, *MNRAS*, 271, 247
- Simpson, C., Ward, M., & Kotilainen, J. 1994, *MNRAS*, 271, 250
- Storchi-Bergmann, T., Mulchaey, J. S., & Wilson, A. S. 1992a, *ApJ*, 395, L73
- Storchi-Bergmann, T., Wilson, A. S., & Baldwin, J. A. 1992b, *ApJ*, 396, 45
- Storchi-Bergmann, T., Wilson, A. S., & Baldwin, J. A. 1996, *ApJ*, 560, 252
- Strecker, D. W., Erickson, E. F., & Witteborn, F. C. 1979, *ApJS*, 41, 501
- Turner, T. J., Urry, C. M., & Mushotzky, R. F. 1993, *ApJ*, 418, 653
- Turner, T. J., George, I. M., Nandra, K., & Mushotzky, R. F. 1997a, *ApJS*, 113, 23
- Turner, T. J., George, I. M., Nandra, K., & Mushotzky, R. F. 1997b, *ApJ*, 488, 164
- Turner, T. J., George, I. M., Nandra, K., & Mushotzky, R. F. 1998, *ApJ*, 493, 91
- Wanders, I., et al. 1995, *ApJ*, 453, L87
- Ward, M. J. 1996, in Harris D. E., Carilli C. L., eds. *Cygnus A: Study of a Radio Galaxy*. CUP, Cambridge, p. 43
- Wilson, A. S., & Tsvetanov, Z. I. 1994, *AJ*, 107, 1227

Wood, K. S., et al. 1984, ApJS, 56, 507

Table 1: Near-infrared magnitudes for NGC 3281.

Telescope/Filter	λ (μm)	$m(6'')$	m_{nucleus}	S_{nucleus} (mJy)	
ESO/ <i>J</i>	1.25	12.36			
ESO/ <i>H</i>	1.65	11.46	14.72 ± 0.17	$1.3 \pm$	0.2
ESO/ <i>K</i>	2.20	10.88	12.33 ± 0.10	$7.7 \pm$	0.8
SAAO/ <i>L</i> ^a	3.45	9.11	9.54 ± 0.18	$44.3 \pm$	8.0
UKIRT/ <i>K</i>	2.20	10.82			
UKIRT/ <i>L'</i>	3.80	8.35	8.47 ± 0.09	$103.1 \pm$	9.3
UKIRT/ <i>M</i>	4.80	7.24	7.27 ± 0.12	$207.1 \pm$	24.9

^aFrom Glass & Moorwood (1985).

Table 2: ASCA observations of NGC 3281.

Detector	Exposure time (s)	Source count rate (s^{-1})	Background count rate (s^{-1})
SIS0	14 933	0.0189 ± 0.0015	0.0123 ± 0.0004
SIS1	14 869	0.0156 ± 0.0015	0.0110 ± 0.0003
GIS2	15 310	0.0166 ± 0.0015	0.0092 ± 0.0002
GIS3	15 342	0.0204 ± 0.0017	0.0108 ± 0.0002

Table 3: Fits to the X-ray data. Uncertainties quoted are 90% confidence intervals.

Parameter	All	SIS0+SIS1	GIS2+GIS3
All data			
χ^2/ν	63.57 / 68	23.68 / 30	20.29 / 34
Γ	$2.18^{+0.30}_{-0.29}$	$2.55^{+0.36}_{-0.37}$	$1.67^{+0.45}_{-0.48}$
N_{H} (10^{26} m^{-2})	$75.8^{+11.6}_{-10.6}$	$67.8^{+9.0}_{-10.1}$	$93.3^{+28.4}_{-22.8}$
$\text{EW}_{\text{Fe K}\alpha}$ (eV)	430^{+470}_{-210}	320^{+400}_{-190}	730^{+1660}_{-480}
$E > 1 \text{ keV}$			
χ^2/ν	50.66 / 59	12.36 / 21	20.07 / 33
Γ	$1.82^{+0.37}_{-0.26}$	$2.06^{+0.87}_{-0.72}$	$1.69^{+0.55}_{-0.46}$
N_{H} (10^{26} m^{-2})	$72.5^{+12.5}_{-12.0}$	$64.7^{+13.3}_{-11.6}$	$88.9^{+26.8}_{-21.3}$
$\text{EW}_{\text{Fe K}\alpha}$ (eV)	480^{+770}_{-230}	260^{+900}_{-230}	730^{+2100}_{-500}

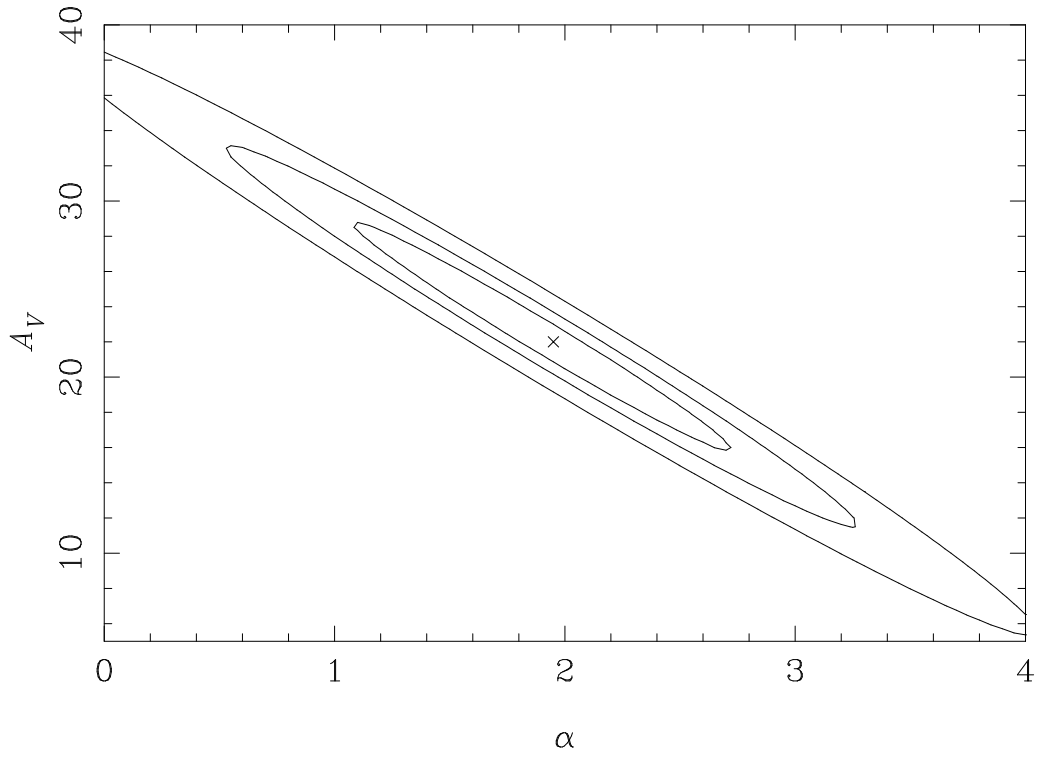


Fig. 1.— Confidence contours in the spectral index–extinction plane for fitting a reddened power law to the nuclear fluxes. The cross marks the minimum of χ^2 , and the contours are at 68%, 90%, and 99% confidence intervals. Spectral index is defined in the sense $S_\nu \propto \nu^\alpha$.

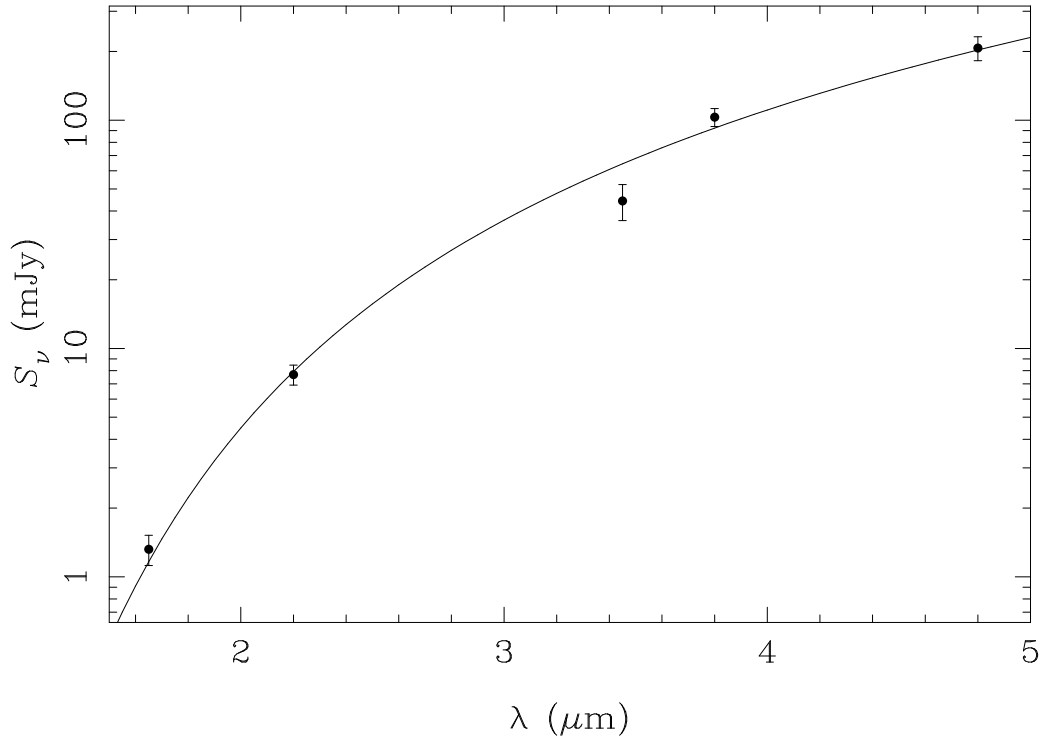


Fig. 2.— The measured fluxes of the nuclear source in NGC 3281 (points with error bars) and the best fit reddened power law (solid line), as determined by the analysis of Figure 1.

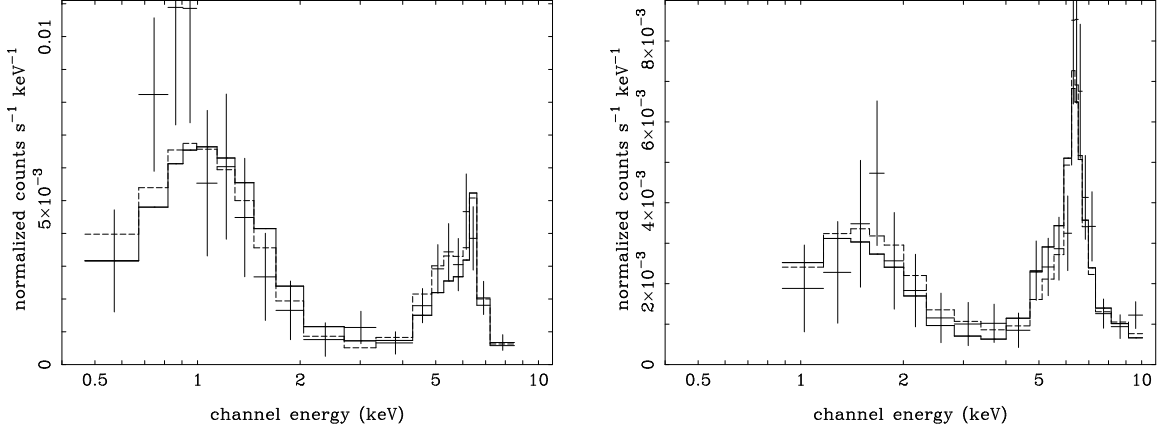


Fig. 3.— Data from the SIS0 (left) and GIS3 (right) detectors, together with the best fit model obtained from fitting (solid lines) all 4 detectors simultaneously, and (dashed lines) each pair of detectors only (i.e. SIS0+SIS1 or GIS2+GIS3).

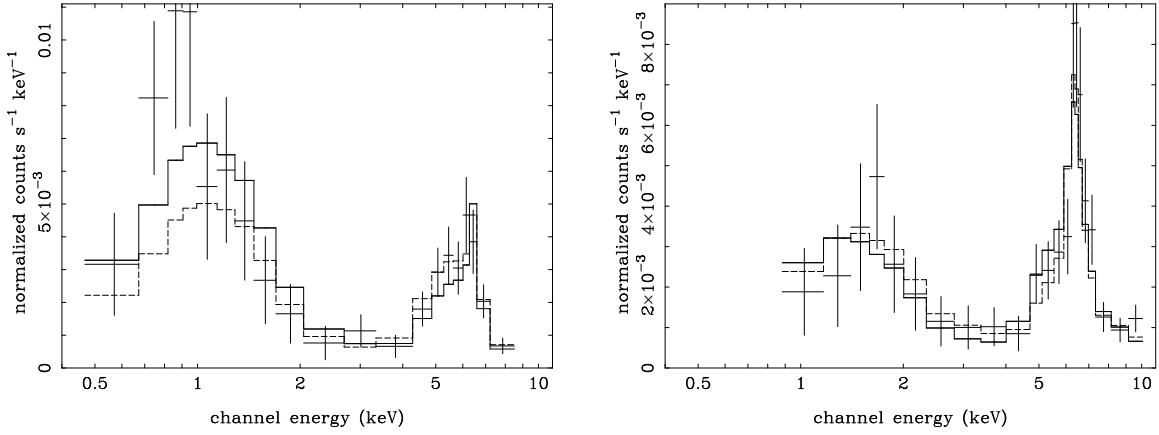


Fig. 4.— Data from the SIS0 (left) and GIS3 (right) detectors, together with the best fit model for the data at energies above 1 keV obtained from fitting (solid lines) all 4 detectors simultaneously, and (dashed lines) each pair of detectors only (i.e. SIS0+SIS1 or GIS2+GIS3).

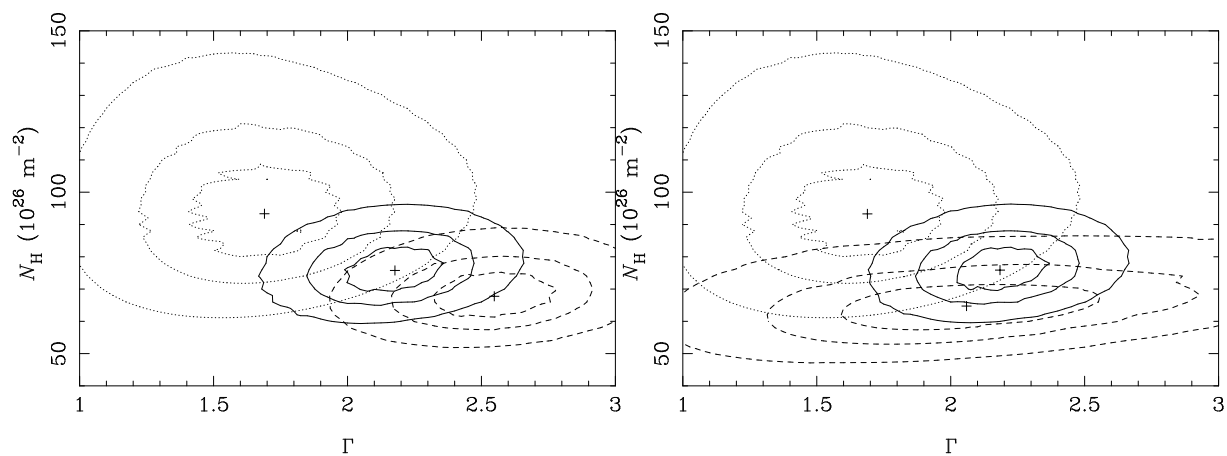


Fig. 5.— Photon index–hydrogen column density confidence contour plots for the entire energy range (left) and energies above 1 keV only (right). The crosses mark the locations of the best fits (see Table 3), and the contours are at 68%, 90% and 99% confidence. Solid lines are confidence contours for the simultaneous fits to all four detectors, dashed lines for fits to the SIS0+SIS1 detectors, and dotted lines for the GIS2+GIS3 detectors.

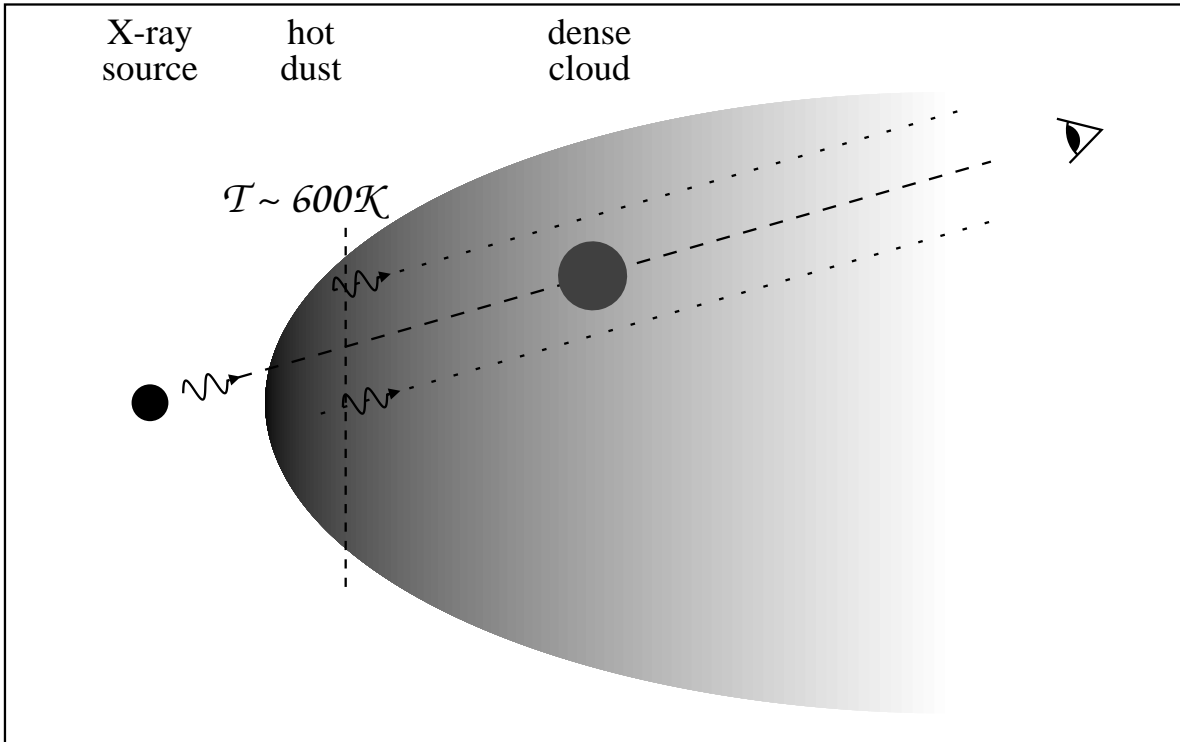


Fig. 6.— Schematic diagram showing how a dense cloud located within the torus can explain the very large $N_{\text{H}}/A_{\text{V}}$ ratio we measure in NGC 3281. The line of sight to the X-ray source (long dashed line) passes through a dense cloud with a high column density, while much of the infrared-emitting hot dust suffers much lower obscuration (short dashed lines).